Icarus 378 (2022) 114914

Contents lists available at ScienceDirect

Icarus

journal homepage: www.elsevier.com/locate/icarus

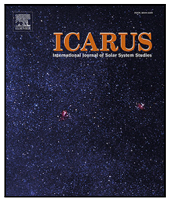

Letter

Interior of top-shaped asteroids with cohesionless surface

Fabio Ferrari [a,*], Paolo Tanga [b]

[a] Physics Institute, University of Bern, Switzerland
[b] Universitè Côte d'Azur, Observatoire de la Côte d'Azur, CNRS, Laboratoire Lagrange, France

ARTICLE INFO

Keywords:
Asteroids
Asteroids, dynamics
Asteroids, surfaces
Interiors

ABSTRACT

Multiple sources of evidence suggest that asteroids ranging from hundreds meters to few kilometers in size are rubble piles, i.e. gravitational aggregates of loosely consolidated material. However, no direct data on their internal structure is available to date. Cohesion between rubble-pile building blocks has been invoked in the past to explain the stability of top-shaped asteroids, which in most cases would not be capable of maintaining their large-scale shape features (low flattening, and a pronounced equatorial ridge) otherwise. However, the physical origin of cohesion is unclear and there is no direct evidence of it. Recent close-range imaging and local sampling of the surfaces of top-shaped Near Earth Asteroids (NEA) suggest the presence of very porous surface structure with minimal strength and nearly no cohesion. This raises new questions about the internal structure of such objects, with important implications on their origin and evolution. Here we show by numerically simulating the dynamics of irregular rocky fragments, that the presence of a rigid core within the asteroid's rubble-pile structure can explain the top shape and surface features observed recently on Bennu and Ryugu, without the need of cohesion between building blocks. Also, we find that the rigid core model produces more easily equatorial mass shedding, which is thought to be responsible for satellite formation. The presence of a rigid core has never been revealed so far, but is consistent with the accretion history of those objects, and with recent estimates of their internal mass distribution. Our findings will be tested directly by ESA's Hera mission, which will scan the interior of Dimorphos, the small moon of Didymos binary system, providing for the first time direct data on the interior of a NEA.

1. Introduction

Recent in-situ observation of JAXA's Hayabusa 2 and NASA's OSIRIS-Rex (Origins, Spectral Interpretation, Resource Identification, Security, Regolith Explorer) missions revealed both characteristic and unexpected features of asteroids Ryugu and Bennu respectively. Both asteroids are characteristic top-shaped rubble piles, with very high levels of porosity (40%–60%) and a prominent equatorial bulge (Watanabe et al., 2019; Lauretta et al., 2019a). At the same time, both asteroids show unexpected features. Their surface is covered with highly porous rocky material, with high abundance of boulders, little amount of fine-grained regolith and nearly no cohesion between grains (Barnouin et al., 2019; Walsh et al., 2019; Sugita et al., 2019; Morota et al., 2020; Arakawa et al., 2020; Ho et al., 2021). Measures of Bennu's proximity gravity field have revealed a heterogeneous mass distribution, whose deviations are consistent with lower densities towards its center and equatorial bulge (Scheeres et al., 2020, 2019). However, the geophysics and internal structure of these objects remains poorly constrained and largely unknown due to the lack of direct measurements (Herique et al., 2018; Murdoch et al., 2015; Hestroffer et al., 2019).

In the past decades, the absence of such data has fostered the development and consolidation of numerical simulations, as a crucial tool to investigate the origin, evolution and internal structure of small celestial bodies (Asphaug and Benz, 1994; Leinhardt et al., 2000; Michel et al., 2001, 2003; Jutzi et al., 2013; Sugiura et al., 2021). The rubble-pile nature of these objects makes their dynamics suitable to be simulated using DEM (Discrete Element Method) codes, as gravitational aggregates of boulders and pebbles interacting through self-gravity and contact/collisions. When paired with remotely observable quantities and in-situ measures, numerical simulations provide an indispensable mean to test hypotheses on rubble-piles internal structures. Examples of this approach are found in recent advances of the understanding of the formation and dynamical evolution of asteroids (e.g., Walsh et al., 2008; Michel et al., 2020; Hirabayashi et al., 2019, 2020; Yu et al., 2018; Zhang and Lin, 2020; Campo Bagatin et al., 2020).

In the context of the theory of continuum, Holsapple (2004) showed that most asteroid shapes can be explained by the effect of friction only. However, when applied to rubble-pile asteroids, i.e., gravitational aggregates, the theory of continuum relies on major simplifications,

* Corresponding author.
E-mail address: fabio.ferrari@unibe.ch (F. Ferrari).

https://doi.org/10.1016/j.icarus.2022.114914
Received 6 October 2021; Received in revised form 21 January 2022; Accepted 24 January 2022
Available online 7 February 2022

which leads to inaccurate treatment of such granular systems. In this context (e.g., when modeling rubble piles using granular DEM N-body codes), the nonhydrostatic shape of many known top-shaped asteroids, as well as the surface features observed by OSIRIS-REx and Hayabusa 2 on Bennu and Ryugu, have been explained in the past invoking a cohesive binding force between rubble-pile constituents (Richardson et al., 2009; Scheeres et al., 2010; Rozitis et al., 2014; Zhang et al., 2018). While cohesion in solid bodies can be defined as shear strength at zero pressure (Holsapple, 2007), in the case of fragmented bodies, this translates into a non-zero tensile strength between rubble-pile fragments. In this context, Scheeres et al. (2010) identified the possible physical origin of cohesion in the presence of van der Waals cohesive forces, which in the asteroid environment might contribute significantly to the evolution of asteroid surfaces and interiors. The current numerical models, however, show that the global stability of the top-shape and the main surface features (e.g., local slopes and equatorial bulge) depend critically on cohesion (Sánchez and Scheeres, 2014, 2018; Leisner et al., 2020; Zhang et al., 2021), poorly known in both its intensity and origin. The widespread presence of top-shaped Near Earth Asteroids apparently indicates that such critical cohesion is often occurring on their surfaces, but could also suggest that a more general mechanism may exist. Moreover, the response of the surface to the mechanical solicitation during sampling maneuvers, as well as the close observation of surface morphology, has suggested that a cohesion, if present, must be very weak (Barnouin et al., 2019; Sugita et al., 2019; Morota et al., 2020; Arakawa et al., 2020; Ho et al., 2021). To cope with these observations, we investigate here the problem of cohesionless aggregates.

We provide here a new explanation to the presence of surface features and global shape observed in top-shaped asteroids, regardless of exact cohesive properties of material. We take profit of a recent advance in numerical modeling of the rubble-pile problem, exploiting the capability of the GRAINS code (Ferrari et al., 2017, 2020) to handle non-spherical fragments. Compared to spheres, the use of angular particles enhances greatly the realism of contact/collision interactions between building blocks (Ferrari and Tanga, 2020). These are capable to reproduce physical effects due to the geometry of contact interactions, such as interlocking, off-center collisions and particle spin motion (Korycansky and Asphaug, 2006, 2009). In this work we build high resolution models of top-shaped rubble-pile asteroids and study their stability using realistic angular fragments.

2. Methods

We use GRAINS (Ferrari et al., 2017), a N-body DEM code, fully integrated with the multi-physics engine Chrono (Tasora and Anitescu, 2010; Tasora et al., 2016; Mazhar et al., 2013). Self-gravity interactions between fragments are handled in GRAINS by using either direct N-body integration or a GPU-parallel implementation of the Barnes–Hut octree method (Ferrari et al., 2020; Barnes and Hut, 1986; Burtscher and Pingali, 2011). In our simulations, we use the octree when N > 10,000, and direct N-body when N < 10,000. Contact interactions are resolved using the Smooth-Contact Method (SMC) implemented in Chrono (Fleischmann et al., 2015). SMC is a soft-body contact method, similar to the soft-sphere method implemented in other N-body DEM codes (Sánchez and Scheeres, 2011; Schwartz et al., 2012). Simulation parameters are set based on previous studies and benchmarking efforts, to be representative of gravel-like material (Ferrari et al., 2017; Pazouki et al., 2017; Fleischmann et al., 2015). In particular, normal and tangential stiffness coefficients are set to $K_n = K_t = 2 \times 10^5$ N/m, while damping coefficients are set to $G_n = 20$ Ns/m and $G_t = 40$ Ns/m. Coulomb friction is enforced at contact points and we use a friction coefficient of 0.6. We do not consider any cohesive force between fragments. All particles have a non-spherical, irregular shape. Individual shapes are different for each fragment: the shape is generated randomly as the convex envelope of a cloud of points, each having a random position within a cube. As a result, fragments have ~10 vertices on average and aspect ratio (smaller to larger size ratio) between ~0.7 and ~1. The shape of particles is independent on their size, which is varied by scaling up/down the fragment while preserving its shape. As for fragment size distribution, we consider both monodisperse and polydisperse with power law distribution, with an exponent of −2.70 (e.g. Elek and Jaramaz, 2008; Jutzi et al., 2019). More details on the effects of non-spherical particle shapes and their combined effects with friction coefficient are provided in Ferrari and Tanga (2020).

We address the problem of global shape and surface stability by investigating the internal structure and evolution of rubble-pile objects. The analysis builds upon a large dataset obtained from an extensive numerical simulation campaign. We performed several (82 overall) N-body simulations to reproduce the dynamics of representative rubble-pile aggregates with a range of different internal structures, and subject to different evolution histories. As a result, we analyze the properties of the aggregate as it settles to equilibrium. The aggregate is considered in equilibrium when the variation of its principal inertia moments is bounded to less than 1% within several rotation periods of the aggregate. In this case, the shape variation is minimal, lower than the model's minimum particle size. We consider top-shaped rubble piles including asteroid Bennu, to support direct comparison with OSIRIS-Rex observations, and the primary of Didymos system, the target of upcoming NASA's DART (Double Asteroid Redirection Test) (Cheng et al., 2018) and ESA's Hera (Michel et al., 2018) missions. Also, we adopt tri-axial ellipsoids to reproduce objects with a more regular surface. We use the triangulated shape model for Bennu (Barnouin et al., 2019) and Didymos (Naidu et al., 2020) and three tri-axial ellipsoid models representative of Didymos' moon Dimorphos (Pravec et al., 2016): in the followings, these are referenced as Dimorphos(1), with semi-axes ratios a/b = 1.2, b/c = 1.1; Dimorphos(2), with a/b = 1.3, b/c = 1.2; and Dimorphos(3), with a/b = 1.4, b/c = -1.3. Note that in the case of Dimorphos we simulate the full binary environment, taking into account the gravity of the primary as a point-mass source, and the full orbital/rotation motion of Dimorphos around the barycenter of Didymos system. The rubble-pile DEM models are built by gravitational accretion and set to match the shape and physical properties of the asteroid, using the methodology reported in Ferrari and Tanga (2020). Several rubble-pile models of Bennu, Didymos and Dimorphos are built, to account for different fragment size distribution (monodisperse and polydisperse) and different internal structure, using between 1600 and 20,000 particles. The number of particles is chosen as a result of a trade-off between computational effort and model resolution. However, improving the resolution is very slow for increasing N, whereas computational effort grows rapidly. For example, the monodisperse 10k-particle model of Bennu has a resolution of 5.7 m, and increasing N by one order of magnitude (up to 100k particles) results in a resolution of 2.6 m (nearly twice as better), at the cost of a much higher computational time, which scales with N^2 (or $N \log N$ in case the octree is used). As for the internal structure, we explore three main cases: (a) homogeneous rubble-pile, where the aggregate is fully fragmented with a homogeneous density distribution, (b) two-layer rubble-pile, where the aggregate is fully fragmented but with a non-homogeneous density distribution to account for higher/lower density layers, and (c) rigid core rubble-pile, with a inner rigid core made of one or few big boulders surrounded by a thick layer of fragments. For the layered case, density distribution is adjusted by changing material density of the particles, while keeping the overall bulk density constant. The total bulk density of rubble-pile models of Bennu are set to its observed value of 1.19 g/cm^3 (Barnouin et al., 2019). Due to the large uncertainty in Didymos' bulk density (2.17 ± 0.35 g/cm^3, Naidu et al., 2020), we consider both nominal (2.17 g/cm^3) and upper bound (2.52 g/cm^3) cases. For the case of heterogeneous density models (both of Bennu and Didymos), we investigate the effect of different density values within each layer, including both denser and underdense cores (Scheeres et al.,

2020). The mean resolution of our rubble pile models is in the order of ∼5–10 m, with smaller fragments down to few meters in size and larger surface boulders up to ∼70 m. We investigate rubble piles with rigid cores of various sizes consisting in up to 50% of the asteroid's volume, down to fully fragmented aggregates (Hirabayashi et al., 2015; Cheng et al., 2020). In terms of dynamical scenarios, we simulate the dynamics of these rubble-pile models under different evolution patterns: (a) formation, where the aggregate is formed and settled at the asteroid's nominal spin, (b) slow spin-up, where the aggregate is formed and settled at zero spin and then spun-up quasi-statically (i.e., $\Delta\omega < 1\%$ of the nominal spin) to its nominal spin and (c) fast spin-up, where the aggregate is formed and settled at zero spin and then spun-up abruptly to nominal spin (i.e., $\Delta\omega > 10\%$ of the nominal spin). These would be representative of scenarios where (a) the asteroid does not undergo any major reshaping after formation, (b) slow change of spin due to Yarkovsky–O'Keefe–Radzievskii–Paddack (YORP) effect (Rubincam, 2000), (c) abrupt change of spin due to e.g. collisions (Paolicchi et al., 2002).

3. Results

3.1. Qualitative behavior

Simulation results show that the presence of a rigid core inside the rubble-pile structure enhances greatly the stability of the global shape and surface features of the object. This is in agreement with previous results by Hirabayashi (2015), but with the difference that we do not provide any cohesion between fragments. The term "rigid core" indicates here the presence of a large amount of rigid volume within the internal structure. This could be provided by a single monolithic block, or by multiple large blocks. For this reason, to identify the size of the inner core, we refer to its *volume*, rather than to its *radius*. This consideration was suggested by the results of our simulations, which show that the amount (percentage) of rigid volume within the internal structure of the aggregate is more important than the geometrical configuration of the core (whether this is made of one or more blocks), when assessing the stability of the rubble pile. In fact, while the geometrical configuration has some effect on the transient dynamics during failure and reshaping, it has nearly no effect on the global stability versus instability of the aggregate.

The effects of a rigid interior on the global shape and surface features of a rubble-pile aggregate are shown in Fig. 1. The final equilibrium configurations (right column) of four simulated rubble-pile aggregates are compared. Each row of Fig. 1 shows the time evolution of the aggregate as it deforms towards equilibrium. At initial time (left column), the four rubble-pile objects have the same shape, bulk density and spin rate, but different internal structure. In this case, we show the Didymos case study, with a single monolithic inner core. The size of the inner core decreases from top to bottom, down to a fully fragmented model with no rigid core (bottom row). Irregular global features such as the equatorial bulge appear only when the rigid inner core is present and sufficiently large. The bigger the core, the more definite is the equatorial bulge, up to a critical size where the bulge breaks up into a ring-like structure of particles orbiting around the central body. In this case the remainder of the aggregate is markedly top-shaped, with sharp equatorial edges. As a general result, we observe smooth and regular surfaces on fully fragmented objects, i.e., with no rigid core, and vice versa: ridges and other topographical irregularities are observed on aggregates with rigid and large inner cores. As mentioned, when assessing the stability of the global shape and surface features, we do not observe any major difference due to the shape of the rigid core, or due to the core being made of a single monolith or few big blocks. Instead, the stability properties depend directly on the amount of fragmented vs rigid internal volume. Although not affecting the global stability of the aggregate, the geometrical configuration of the rigid volume and the presence of one or more rigid blocks, is observed to affect the local mass flows within the internal structure and surface of the aggregate. As expected, the overall bulk density of the aggregate plays a role in assessing the overall stability of the aggregate (Holsapple, 2004). Instead, we do not observe any relevant difference between models with a different heterogeneous density distribution and an equal bulk density, which seems to be the only critical parameter. From the shape and surface stability point of view, having a denser or underdense core plays a minor role, if the overall bulk density is preserved, and if the core is not rigid.

For the case of Didymos with nominal bulk density, the minimum rigid internal volume to maintain irregular surface features is quantified in the range ∼10%–25% of the asteroid's total volume. Below this value, equilibrium aggregates show smooth and regular ellipsoidal shape. Mass shedding is observed to be facilitated both by larger rigid volume fraction and by a fast spin-up history. In the formation scenario, mass shedding is observed in aggregates with inner rigid volume fraction greater than ∼25%, and no mass ejection is observed with a lower rigid fraction. Didymos is estimated to be stable at its nominal spin for an inner rigid fraction sensibly greater than ∼50%. For reference, the size of the cores in Fig. 1 is (from top to bottom row) approximately 50%, 25% and 10% (bottom row case has no rigid core) and none of these cases are shown to be stable.

A similar pattern is observed for simulation cases considering models of asteroid Bennu. Fig. 2b and Fig. 2c show two rubble-pile models of Bennu, constructed using 10k fragments of irregular shape, with polydisperse (b) and monodisperse (c) grain size distribution. The mean fragment size of rubble-pile models is ∼6 m (monodisperse) and ∼8 m (polydisperse, in this case the minimum fragment size is ∼2 m and the largest boulders are up to ∼35 m in size). For comparison, we show the image of Bennu from OSIRIS-REx observations in Fig. 2a. We simulate the dynamics of Bennu as a rubble pile, using both a fully fragmented interior and a rigid internal core. Red and yellow lines in Fig. 2a show the envelope of the equilibrium shapes for the fully fragmented interior (red) and for the aggregate with rigid core (yellow). We observe that an internal rigid volume of about 50% of Bennu's total volume, is sufficient (with no cohesion needed in the external layers) to stabilize the global shape of Bennu and its surface features, which instead are not stable in the fully fragmented case. In the latter case, the equilibrium shape is flattened at the poles and has a higher radius both at equatorial and mid latitudes, with a ratio of 0.79 between the polar and maximum equatorial radii, sensibly lower than 0.90 of Bennu's observed shape (Barnouin et al., 2019). Instead, the equilibrium shape of Bennu's model with rigid core is very consistent with observed shape. For direct comparison, we report the detailed topographic information of Bennu's rigid-core model simulated with GRAINS in Fig. 3. The local surface radius shown in Fig. 3(a–d) closely matches that of Bennu, with low flattening, low mid-latitude radius, and prominent equatorial ridge. Fig. 3(e–h) illustrates the local altitude with respect to the longitudinally-averaged radius, showing that the longitudinal ridges observed by OSIRIS-REx (Barnouin et al., 2019) are preserved in our model. Consistently with Bennu's observations, the longitudinal ridges contribute to the diamond-shaped equatorial profile of the aggregate, and their four main equatorial signatures are equally spaced at roughly 90 deg angular distance, as shown in Fig. 3(i–j).

In all simulations, we observed that characteristic time scales to reach a stable configuration depend mainly on the dynamical scenarios involved. All asteroids in the formation or spin-up scenarios settle quite rapidly to equilibrium, after a few spin periods only. This is different by construction, for slow spin-up scenarios, which imply much longer simulations, in order to let the aggregate spun-up quasi-statically. On the other hand, a relevant difference is found in simulations where mass shedding occurs. In these cases the time to reach a stable configuration is substantially increased due to motion of shed material.

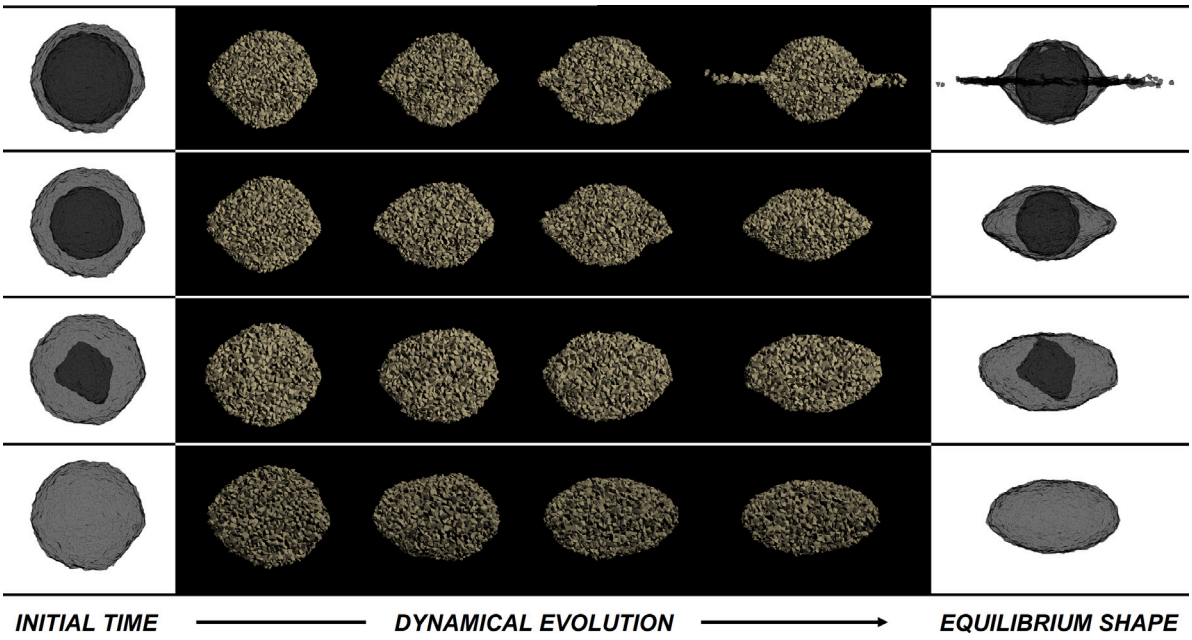

Fig. 1. N-body simulations of rubble-pile aggregates with GRAINS. All aggregates are shown in their side view, with spin vector in the vertical direction. Each row shows the time evolution of the initial aggregate (left column) as it deforms towards its equilibrium shape (right column). We show the internal structure of initial and final aggregates, with inner rigid core surrounded by a transparent layer of fragmented material (left and right columns, white background), while the external rocky surface is shown during the dynamical transient (black background, middle columns). Four simulations are shown for the case of Didymos: all initial aggregates share the same spin conditions, same initial shape, same bulk density, but different internal structure. The size of rigid core decreases from top to bottom, which has no inner core. The final configurations (right) reveal a correlation between the equilibrium shape, the existence of irregular surface features and the size of the inner core.

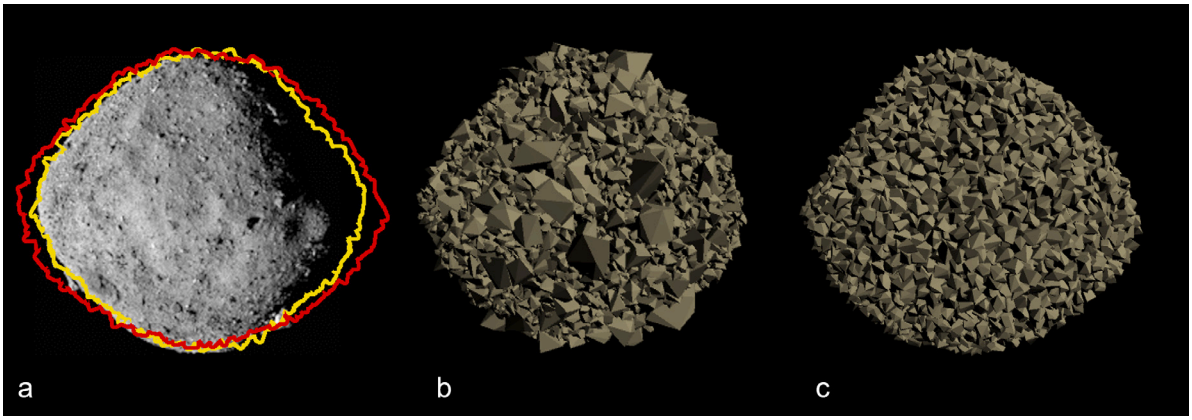

Fig. 2. a: Asteroid Bennu from OSIRIS-REx observations. Red and yellow lines are the envelope of equilibrium shapes obtained using rubble-pile models of Bennu with fully fragmented interior (red) and with inner rigid fraction of ~50% (yellow). b–c: Rubble-pile model of asteroid Bennu using 10k irregular fragments with polydisperse (b) and monodisperse (c) size distribution. The mean fragment size of rubble-pile models is ~6 m (c) and ~8 m (b, in this case the minimum fragment size is ~2 m and the largest boulders are up to ~35 m in size). (For interpretation of the references to color in this figure legend, the reader is referred to the web version of this article.)
Source: Mosaic, credit: NASA/Goddard/University of Arizona.

3.2. Quantitative assessment

The main results and qualitative behavior are summarized above. In addition, we provide here a more systematic analysis of simulation results. To this goal, we propose here two metrics to measure quantitatively the irregularity of both surface and global shape of the aggregate after it settles to equilibrium. First, we introduce the *Index of Smoothness* (IoS), defined as

$$\mathrm{IoS} = 1 - \frac{S_\mathrm{e}}{S} \tag{1}$$

where S is the total surface area enveloping the final aggregate and S_e is the surface area of the Dynamically Equivalent Equal Volume Ellipsoid (DEEVE), having the same moments of inertia and volume of the numerically computed aggregate. The IoS provides a measure of how the surface of the body is irregular, compared to the smooth surface of the equivalent ellipsoid. In principle, any surface irregularity, such as ridges, grooves, mountains and canyons contribute to increase the overall surface area of the object with respect to a smooth ellipsoidal surface. Therefore $S > S_\mathrm{e}$ for any real, non-perfectly smooth object, with IoS ranging from 0 (perfectly smooth surface), to 1 (asymptotic value for extremely irregular surface, with $S \gg S_\mathrm{e}$). For our case of study (aggregates with nearly ellipsoidal or top shapes) the IoS proved indeed to be a good measure of the level of surface irregularity. The second index is borrowed from the theory of continuum (Chandrasekhar, 1969), and in particular from its application to non-fluid bodies with a non-zero angle of friction (Holsapple, 2004). In detail, we compute the minimum angle of friction required to maintain the aggregate's shape, according to the Drucker–Prager limiting failure condition (see Ferrari and Tanga, 2020, for further details on implementation). In this work,

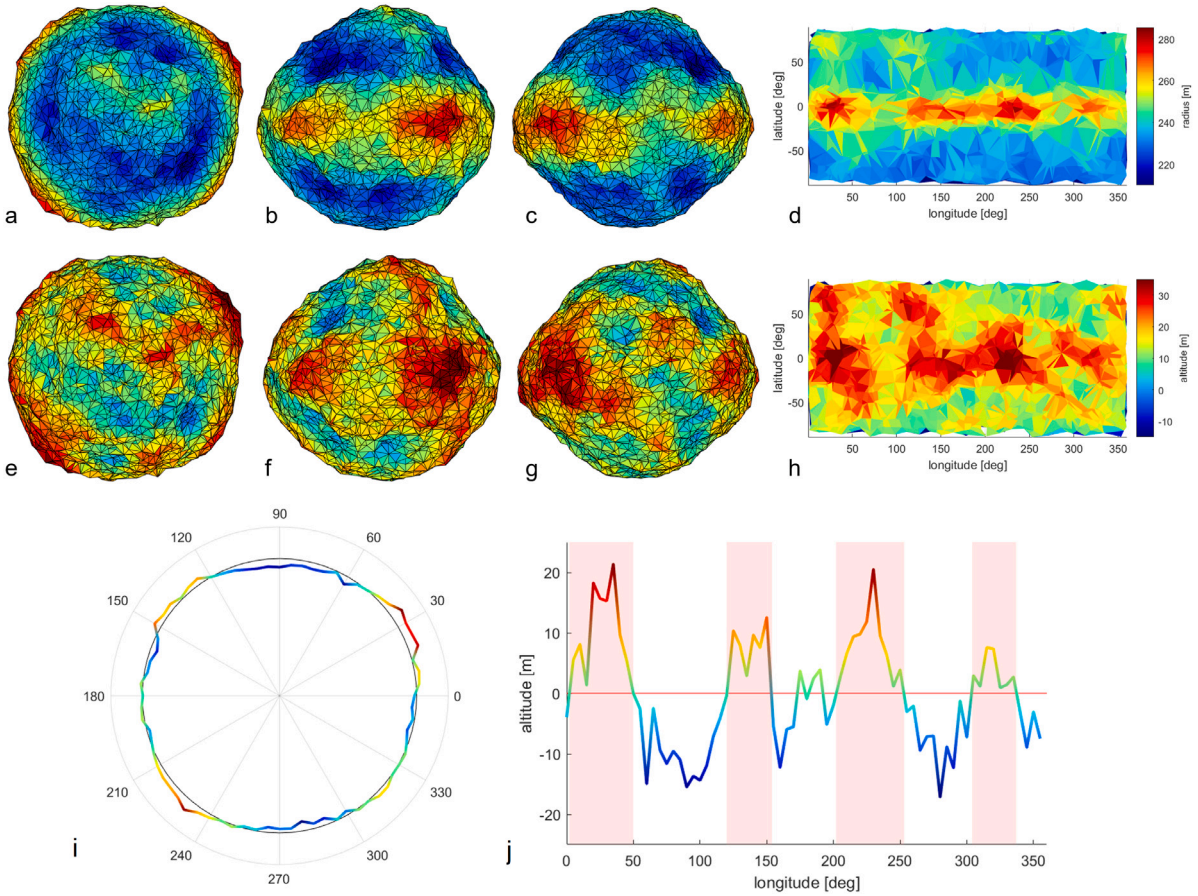

Fig. 3. Topographic maps of a Bennu-shaped aggregate with inner rigid fraction of ∼50%. Local surface radius (a–d) and altitude with respect to the longitudinally averaged radius (e–h) are shown in north pole views (a, e), side views from 0 deg (b, f) and 270 deg longitude (c–g) and 2D latitude–longitude map (d–h). i–j: Topographic altitude at equator with respect to the longitudinally averaged equatorial radius. i: north pole view of the equator and deviation from longitudinally averaged equatorial radius. j: altitude deviation as function of the longitude. Red and shaded regions are elevated above the mean equatorial radius. Four main elevated regions are observed, spaced roughly by 90 deg in longitude. (For interpretation of the references to color in this figure legend, the reader is referred to the web version of this article.)

the Drucker–Prager minimum theoretical angle of friction (also θ_{DP} in the following) is used as measure of how far the aggregate's equilibrium shape is from its theoretical hydrostatic equilibrium one. A value of $\theta_{DP} = 0$ implies that the aggregate is at a hydrostatic equilibrium condition, i.e., its shape that can be withstood by a fluid body with zero angle of friction (for an incompressible, constant-density body). In our case, for a granular non-fluid aggregate, $\theta_{DP} > 0$.

Aggregated plots of results, considering all simulations performed, are reported in Fig. 4. These provide basic relations between key properties of the final aggregate, such as surface irregularity (IoS), shape irregularity (θ_{DP}), mass shed (if any, M_s) and percentage of inner rigid volume (V_r, proportional to the size of the marker in the plots). The role of the inner core and its correlation to surface/shape irregularity emerges clearly from the data. In addition, we report observed trends and relations between key parameters of the problem. Some of these provide interesting insights and would deserve a dedicated analysis, which however is out of the scope of this paper.

Fig. 4 confirms the general qualitative description provided above. In particular, irregular surfaces are observed in aggregates with rigid core only. Figs. 4(a) and 4(b) show that the measured IoS is always lower than 0.25 for fully fragmented aggregates. This suggests that full rubble piles can hardly withstand irregular surfaces, which instead are observed on aggregates with rigid core, where the value of the IoS is higher and ranges up to 0.5. In addition, Fig. 4(a) shows that fully fragmented bodies are more likely to form aggregate shapes close to hydrostatic equilibrium (low θ_{DP}), with smooth surfaces (low IoS). Aggregates with rigid core appear to be clustered in two branches (Fig. 4(a)), with the majority of them populating the right branch, where surface irregularity (IoS) scales approximately linearly with shape irregularity (θ_{DP}). Most noticeably, the higher the percentage of inner rigid volume, the more the surface and shape are irregular. Figs. 4(b) and 4(c) show that mass loss is more likely for aggregates with rigid core. Also, according to Fig. 4(b), the amount of mass shed increases exponentially with IoS, suggesting a correlation between the existence of irregular surfaces and the likelihood of past mass shedding events. Finally, Fig. 4(c) shows a bifurcating V-shape relation between shape irregularity and the amount of mass shed. In our simulations, these appear to be associated to different mass shedding mechanisms: the left branch contains aggregates closer to hydrostatic shape and smaller rigid core, with mass loss from the tips of the lowest inertia axis. On the other side, the right branch contains all top-shaped aggregates, with largest rigid core and equatorial mass loss. Note that logarithmic y-axes in Figs. 4(b) and 4(c) are adjusted to show cases with zero mass shedding. Overall, the quantitative analysis of results confirms that the presence of a rigid core is critical to form aggregates with irregular surface features and with a largely nonhydrostatic shape.

For the sake of completeness, a summary of all numerical simulations performed is reported in the Appendix A: Table 1 reports for each simulation the main input parameters and results, including computed IoS and θ_{DP} of equilibrium aggregates.

4. Discussion

The results of our simulations show a clear correlation between the internal structure, the global shape at equilibrium, and the existence

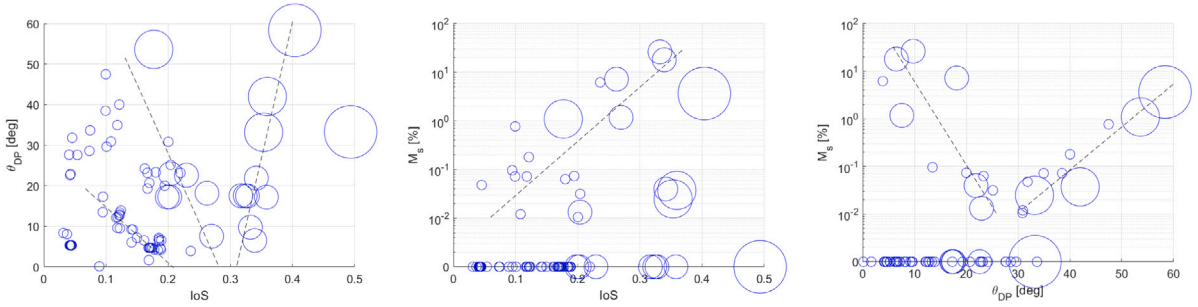

Fig. 4. Aggregated simulation data as function of the Index of Smoothness (IoS), minimum theoretical angle of friction according to the Drucker–Prager criterion (θ_{DP}), percentage of mass shed (if any, M_s), and percentage of inner rigid volume (size of marker, with smaller circles representing fully fragmented aggregates). Data and major trends are shown for all simulations in the (a) IoS-θ_{DP}, (b) IoS-M_s and (c) θ_{DP}-M_s planes. Logarithmic y-axes in (b) and (c) are adjusted to show cases without any mass shedding (with $M_s = 0$).

of irregular features such as equatorial or longitudinal ridges on the surface of a rubble-pile aggregate. These features are observed for aggregates with a rigid core only, and their properties depend on the amount of rigid volume within the internal structure. Top shapes are observed for fast-spinning aggregates with a rigid core. In our simulations, we observe the formation of top shapes through a spin-up process, which in most cases is also followed by mass shedding from the equator. The amount of mass shed is regulated by the spin-up acceleration and final spin rate. When above the critical spin, fast spin-up (due to e.g. impact) results in huge mass shedding, while slow spin-up (due to e.g. YORP) results in tidal saltation (Harris et al., 2009) of particles rolling and bouncing slowly on the surface. This is followed by a slow global reshape with only a few fragments ejected. Also, top shapes are never observed for fully fragmented objects, which form objects with more regular surfaces and shapes closer to hydrostatic equilibrium.

The presence of a rigid core prevents the failure of the internal volume of the aggregate, and allows huge surface movement. Similar motion does not occur in fully fragmented bodies without generating global failure of internal structure. This is similar to what observed by Hirabayashi (2015), but our model does not include any cohesion between fragments. Similar results are also reported by Sánchez (2015), including considerations on the stability of top-shaped rubble piles, which might imply inner rigid cores with a volume fraction comparable to our simulated cases. The fast spin-up scenario is more likely to result in fast and huge mass shedding, which is observed in rubble-piles with a rigid core only. Also, the higher the total mass of the aggregate, the more mass is shed above the critical radius (Hu et al., 2021).

A rigid-core model is possibly consistent with a formation scenario of catastrophic collision and reaccumulation (Michel et al., 2003). In this case it is reasonable to assume a non-uniform size distribution of fragmented material, arranged in a typical power-law fashion, resulting in few very large blocks and many smaller particles. During the reaccumulation process, the larger and more massive blocks act as attractors that could collect smaller fragments around them. The larger blocks would form the inner core of the aggregate. We remark that the rigid core does not have to be monolithic, but might be made of few very large angular boulders locked together through geometrical interlocking and friction.

4.1. Bennu, Ryugu, Didymos

Although no direct measurement of Bennu's interior is available, OSIRIS-REx's observations are consistent with a rigid internal structure, which would be needed to maintain its nonhydrostatic shape and irregular surface features such as its equatorial and longitudinal ridges (Barnouin et al., 2019; Roberts et al., 2021). A heterogeneous mass distribution model is also consistent with Bennu's external gravity field measurements: in a two-layer density model (Scheeres et al., 2020), the central constant-density core would have a radius between 108 to 245 m. We estimate here that ~50% of Bennu's inner volume is rigid. A monolithic, spherical single-block rigid core of such volume would have a radius of about 195 m, which falls within the range estimated by Scheeres et al. (2020). However, Tricarico et al. (2021) estimate that the larger boulder in Bennu's rubble interior may be up to 145 m in size. Therefore, we suggest that the ~50% rigid fraction is shared between multiple large blocks, rather than a single monolith. In addition, Scheeres et al. (2020) suggest that the central core may be underdense with a mass deficit between 6% and 16%. We investigated the effects of denser and underdense cores in heterogeneous density models and we found no relevant difference in the stability properties compared to homogeneous models, as long as the total bulk density remains the same. We do not address here the origin of such underdense region, and we only observe that this does not affect the stability of the global shape and surface features.

Bennu has a rotation period of 4.296 h and is currently undergoing a slow YORP-driven spin-up (Nolan et al., 2019). Our slow spin-up simulation cases show that, in presence of a rigid core, the upper cohesionless layer is subject to slow reshaping, that may lead to moderate particle ejection from the surface, or result in tidal saltation (Harris et al., 2009) of fragments levitating and re-depositing on the surface. This scenario is consistent with evidence of active surface found on Bennu (Jawin et al., 2020; Hirabayashi et al., 2020) and with the episodes of particle ejection captured by OSIRIS-REx (Lauretta et al., 2019b).

Further data elements are provided by the recent exploration of Ryugu, the top-shape rubble-pile asteroid visited by JAXA's Hayabusa 2 mission. As for the case of Bennu, no direct measurement of Ryugu's interior are available. Compared to Bennu, Ryugu has a lower spin rate and is thought to be a at a different stage on its evolutionary process (Hirabayashi et al., 2020). Its shape and topography suggest the asteroid underwent a period of fast spin in its past history (Hirabayashi et al., 2019), which might have led to its top shape. More recently, surface motion has exposed unweathered material at low latitudes and near the equatorial ridge (Morota et al., 2020). Similarly to Bennu, the surface of Ryugu is made of nearly cohesionless material (Sugita et al., 2019; Arakawa et al., 2020; Ho et al., 2021). Based on these similarities and our simulation results, Ryugu's shape and surface features makes it a good candidate to host a inner rigid core.

Compared to Bennu and Ryugu, Didymos primary is estimated to have a higher bulk density (2.1 g/cm3) and a lower rotation period (2.26 h), which locates the object very close to the 2.2 h spin barrier (Naidu et al., 2020). If we assume a cohesionless aggregate, the physical and dynamical properties of Didymos would imply a large rigid core (sensibly larger than 50% of the asteroid's volume), with a shallow outer layer of fragmented material. Such internal structure appears in our simulation as the result of fast spin-up, followed by huge mass wasting which removes a substantial fraction of surface

Table 1
Simulation data: each row represent one full DEM simulation using GRAINS. The initial setup of simulated scenario is provided under *Initial Conditions*. Properties of the aggregate (or its largest remnant in case of mass shedding) after settling at equilibrium are provided under *Equilibrium Aggregate*. $\langle Asteroid \rangle$ shape model and nominal spin used for the simulations. Radar/observation-based models are used for Didymos (primary) and Bennu. Ellipsoidal models are used for Dimorphos with three different axis ratio combinations: Dimorphos(1) a/b = 1.2, b/L = 1.1; Dimorphos(2) a/b = 1.3, b/L = 1.2; Dimorphos(3) a/b = 1.4, b/L = 1.3. $\langle N \rangle$ number of particles in the model. $\langle MPS \rangle$ minimum particle size (resolution of the model). $\langle \rho_b \rangle$ bulk density. Letters indicate the inner density distribution: (H)omogeneous, (L)ayered with inner (D)enser of (U)nderdense core. $\langle V_r \rangle$ percentage of inner rigid volume. $\langle history \rangle$ formation, slow spin-up, fast spin-up. $\langle IoS \rangle$ Index of Smoothness. $\langle \theta_{DP} \rangle$ minimum theoretical angle of friction according to the Drucker–Prager criterion. $\langle M_s \rangle$ percentage of mass shed (if any). Bennu* case (second row in the table) denotes a scenario where Bennu is spun-up above its nominal spin rate, until any mass is shed from its surface.

Initial conditions						Equilibrium aggregate		
Asteroid	N	MPS [m]	ρ_b [kg/m^3]	V_r [%]	History	IoS	θ_{DP} [deg]	M_s [%]
Bennu	10000	2	1190-H	1	slwSP	0.09	0.1	–
Bennu*	10000	2	1190-H	1	slwSP	0.12	40.0	0.2
Bennu	10001	6	1190-H	0	slwSP	0.17	1.7	–
Bennu	10001	6	1190-H	0	form	0.12	12.1	–
Bennu	20000	4	1190-LD	0	form	0.12	12.6	–
Bennu	10001	6	1190-LD	0	form	0.12	12.3	–
Bennu	10001	6	1190-LD	0	form	0.12	12.9	–
Bennu	10001	6	1190-LD	0	form	0.12	13.3	–
Bennu	10001	6	1190-LD	0	form	0.12	13.9	–
Bennu	3054	6	1190-H	50	form	0.49	33.3	–
Didymos	8316	4	2170-H	1	form	0.07	33.6	–
Didymos	8316	4	2520-H	1	form	0.07	28.6	–
Didymos	8316	4	2170-H	1	fstSP	0.09	13.5	0.1
Didymos	8316	4	2520-H	1	fstSP	0.10	17.3	–
Didymos	8316	4	2170-H	1	fstSP	0.10	47.5	0.8
Didymos	8316	4	2520-H	1	fstSP	0.10	29.6	–
Didymos	9497	9	2170-H	0	form	0.16	24.2	–
Didymos	9497	9	2520-H	0	form	0.17	23.2	–
Didymos	9497	9	2170-H	0	fstSP	0.20	25.1	0.0
Didymos	9497	9	2520-H	0	fstSP	0.20	30.8	0.0
Didymos	9497	9	2170-H	0	fstSP	0.24	3.9	6.2
Didymos	9497	9	2520-H	0	fstSP	0.22	23.2	–
Didymos	3043	9	2170-H	50	form	0.40	58.4	3.6
Didymos	6030	9	2170-H	25	form	0.36	42.0	0.0
Didymos	6030	9	2170-H	25	form	0.35	33.2	0.0
Didymos	6030	9	2170-H	25	fstSP	0.18	53.6	1.1
Didymos	6784	10	2170-H	10	form	0.33	17.5	–
Didymos	6784	10	2520-H	10	form	0.20	17.2	–
Didymos	6784	10	2170-H	10	fstSP	0.23	22.6	–
Didymos	6784	10	2520-H	10	fstSP	0.27	7.6	1.2
Didymos	8316	4	2170-LD	1	form	0.04	27.6	–
Didymos	8316	4	2520-LD	1	form	0.04	22.9	–
Didymos	8316	4	2170-LD	1	fstSP	0.11	30.9	0.0
Didymos	8316	4	2520-LD	1	fstSP	0.10	38.5	0.1
Didymos	9497	9	2170-LD	0	form	0.17	20.7	–
Didymos	9497	9	2520-LD	0	form	0.17	19.3	–
Didymos	9497	9	2170-LD	0	fstSP	0.18	23.3	0.1
Didymos	9497	9	2520-LD	0	fstSP	0.19	20.0	0.1
Didymos	6784	10	2170-LD	10	form	0.32	17.5	–
Didymos	6784	10	2520-LD	10	form	0.20	17.2	–
Didymos	6784	10	2170-LD	10	fstSP	0.34	21.9	0.0
Didymos	6784	10	2520-LD	10	fstSP	0.34	6.5	18.0
Didymos	6784	10	2520-LD	10	fstSP	0.26	18.1	7.2
Didymos	8316	4	2170-LU	1	form	0.05	27.6	–
Didymos	8316	4	2520-LU	1	form	0.04	22.6	–
Didymos	8316	4	2170-LU	1	fstSP	0.05	31.8	0.0
Didymos	8316	4	2520-LU	1	fstSP	0.12	34.9	0.1
Didymos	6784	10	2170-LU	10	form	0.32	17.5	–
Didymos	6784	10	2520-LU	10	form	0.36	17.2	–
Didymos	6784	10	2170-LU	10	fstSP	0.20	22.9	0.0
Didymos	6784	10	2520-LU	10	fstSP	0.33	9.7	26.2
Dimorphos(2)	3046	3	2153-H	0	form	0.19	6.3	–
Dimorphos(2)	3046	3	2153-H	0	form	0.18	6.7	–
Dimorphos(2)	3046	3	2153-H	0	form	0.18	7.1	–
Dimorphos(2)	3083	1	2153-H	2	form	0.04	8.1	–
Dimorphos(2)	3083	1	2153-H	2	form	0.03	8.4	–
Dimorphos(2)	3046	3	2153-H	0	form	0.16	6.5	–

(*continued on next page*)

layer, leaving the rigid core surrounded by a shallow rubble layer, and in some cases exposed at the poles. This scenario is consistent with the presence of Didymos' moon Dimorphos, which might have formed after mass shedding from the primary (Walsh et al., 2008). Also, this suggests that Didymos underwent a fast/abrupt spin-up in the past, and might be diagnostic of a large impact. Such event would have triggered a huge and fast mass shedding from the equator. As a result of the reaccumulation process, Dimorphos would be a fully fragmented body, with a more regular hydrostatic shape. Consistently, due to its high spin period (11.93 h), the fully fragmented ellipsoidal model of

Table 1 (*continued*).

Initial conditions						Equilibrium aggregate		
Asteroid	N	MPS [m]	ρ_b [kg/m^3]	V_r [%]	History	IoS	θ_{DP} [deg]	M_s [%]
Dimorphos(2)	3046	3	2153-H	0	form	0.19	6.5	–
Dimorphos(1)	2007	3	2153-H	0	form	0.19	4.6	–
Dimorphos(2)	2000	3	2153-H	0	form	0.15	7.2	–
Dimorphos(1)	2007	3	2153-H	0	form	0.18	4.1	–
Dimorphos(1)	2007	3	2153-H	0	form	0.18	4.3	–
Dimorphos(1)	2007	3	2153-H	0	form	0.19	4.2	–
Dimorphos(2)	2000	3	2153-H	0	form	0.14	6.0	–
Dimorphos(1)	2007	3	2153-H	0	form	0.17	4.7	–
Dimorphos(1)	2007	3	2153-H	0	form	0.17	4.7	–
Dimorphos(1)	2007	3	2153-H	0	form	0.17	4.6	–
Dimorphos(1)	2008	1	2153-H	1	form	0.04	5.3	–
Dimorphos(1)	2008	1	2153-H	1	form	0.04	5.3	–
Dimorphos(1)	2008	1	2153-H	1	form	0.04	5.3	–
Dimorphos(1)	2007	3	2153-H	0	form	0.17	4.7	–
Dimorphos(1)	2007	3	2153-H	0	form	0.17	4.7	–
Dimorphos(1)	2007	3	2153-H	0	form	0.17	4.7	–
Dimorphos(1)	2007	3	2153-H	0	form	0.17	4.7	–
Dimorphos(1)	2008	1	2153-H	1	form	0.04	5.3	–
Dimorphos(1)	2008	1	2153-H	1	form	0.04	5.3	–
Dimorphos(1)	2008	1	2153-H	1	form	0.04	5.3	–
Dimorphos(1)	2008	1	2153-H	1	form	0.04	5.3	–
Dimorphos(3)	1687	3	2151-H	0	form	0.12	9.5	–
Dimorphos(3)	1687	3	2151-H	0	form	0.14	9.2	–
Dimorphos(3)	1687	3	2151-H	0	form	0.14	9.2	–
Dimorphos(3)	1687	3	2151-H	0	form	0.12	9.6	–

Dimorphos is found to be stable in our simulations. Our findings will be tested directly by ESA's Hera mission, which will probe the interior of Dimorphos by means of in-situ radar observations and gravity field determination, providing for the first time direct data on the interior of a NEA (Herique et al., 2019).

We remark that the combined use of high resolution models and non-spherical fragments has helped removing any bias due to e.g., tight spherical packing, which could artificially increase the strength and the stability of the aggregate (e.g. Zhang et al., 2021, and others). Also, it has allowed to reproduce complex dynamical effects, such as the rolling of 6-dof fragments on the aggregate's surface. In this context, surface cohesion is not needed to explain the stability of top shapes and surface features of rubble-pile asteroids with some level of internal rigidity.

CRediT authorship contribution statement

Fabio Ferrari: Study lead, Conceptualization of the study, Interpretation of results, Numerical simulations, Data analysis, Manuscript preparation lead. **Paolo Tanga:** Conceptualization of the study, Interpretation of results, Contribution to manuscript preparation.

Declaration of competing interest

The authors declare that they have no known competing financial interests or personal relationships that could have appeared to influence the work reported in this paper.

Data availability

Part of the data that support the findings of this study are publicly available on Zenodo, with the identifiers doi:10.5281/zenodo.3944129 and doi:10.5281/zenodo.3952131. The rest of the data are available from the corresponding authors upon reasonable request.

Acknowledgments

We thank M. Jutzi for insights and feedback. F. F. acknowledges funding from the Swiss National Science Foundation (SNSF) Ambizione grant No. 193346, and from the European Union's Horizon 2020 research and innovation programme under the Marie Skłodowska-Curie grant agreement No. 800060. This work has been carried out within the framework of the NCCR PlanetS supported by the Swiss National Science Foundation.

Appendix A

Table 1 provides information on the full dataset generated, including all numerical simulations performed with GRAINS and their results. More detail on the physical meaning of parameters listed in the table is provided in Sections 2 and 3.

Appendix B. Supplementary material

Supplementary material is available for this paper in the form of video samples, showing numerical simulations of rubble-pile asteroid spin-up (from Fig. 1) using GRAINS.

Supplementary material related to this article can be found online at https://doi.org/10.1016/j.icarus.2022.114914.

References

Arakawa, M., Saiki, T., Wada, K., et al., 2020. An artificial impact on the asteroid (162173) Ryugu formed a crater in the gravity-dominated regime. Science 368, 67–71. http://dx.doi.org/10.1126/science.aaz1701.

Asphaug, E., Benz, W., 1994. Density of comet Shoemaker-Levy 9 deduced by modelling breakup of the parent 'rubble pile'. Nature 370, 120–124. http://dx.doi.org/10.1038/370120a0.

Barnes, J., Hut, P., 1986. A hierarchical O(N log N) force-calculation algorithm. Nature 324, 446–449. http://dx.doi.org/10.1038/324446a0.

Barnouin, O.S., Daly, M.G., Palmer, E.E., et al., 2019. Shape of (101955) Bennu indicative of a rubble pile with internal stiffness. Nat. Geosci. 12, 247–252. http://dx.doi.org/10.1038/s41561-019-0330-x.

Burtscher, M., Pingali, K., 2011. Chapter 6 - An efficient CUDA implementation of the tree-based Barnes hut n-body algorithm. In: Hwu, W.-m.W. (Ed.), GPU Computing Gems Emerald Edition. In: Applications of GPU Computing Series, Morgan Kaufmann, Boston, pp. 75–92. http://dx.doi.org/10.1016/B978-0-12-384988-5.00006-1, URL: http://www.sciencedirect.com/science/article/pii/B9780123849885000061.

Campo Bagatin, A., Alemañ, R.A., Benavidez, P.G., Pérez-Molina, M., Richardson, D.C., 2020. Gravitational re-accumulation as the origin of most contact binaries and other small body shapes. Icarus 339, 113603. http://dx.doi.org/10.1016/j.icarus.2019.113603, URL: http://www.sciencedirect.com/science/article/pii/S0019103519305809.

Chandrasekhar, S., 1969. Ellipsoidal Figures of Equilibrium. Dover Publications, p. 255.

Cheng, A.F., Rivkin, A.S., Michel, P., et al., 2018. AIDA DART asteroid deflection test: Planetary defense and science objectives. Planet. Space Sci. 157, 104–115. http://dx.doi.org/10.1016/j.pss.2018.02.015.

Cheng, B., Yu, Y., Asphaug, E., et al., 2020. Reconstructing the formation history of top-shaped asteroids from the surface boulder distribution. Nature Astron. 5, 134–138. http://dx.doi.org/10.1038/s41550-020-01226-7.

Elek, P., Jaramaz, S., 2008. Fragment size distribution in dynamic fragmentation: Geometric probability approach. FME Trans. 36, 59–65.
Ferrari, F., Lavagna, M., Blazquez, E., 2020. A parallel-GPU code for asteroid aggregation problems with angular particles. Mon. Not. R. Astron. Soc. 492, 749–761. http://dx.doi.org/10.1093/mnras/stz3458.
Ferrari, F., Tanga, P., 2020. The role of fragment shapes in the simulations of asteroids as gravitational aggregates. Icarus 350, 113871. http://dx.doi.org/10.1016/j.icarus.2020.113871.
Ferrari, F., Tasora, A., Masarati, P., Lavagna, M., 2017. N-body gravitational and contact dynamics for asteroid aggregation. Multibody Syst. Dyn. 39, 3–20. http://dx.doi.org/10.1007/s11044-016-9547-2.
Fleischmann, J., Serban, R., Negrut, D., Jayakumar, P., 2015. On the importance of displacement history in soft-body contact models. J. Comput. Nonlinear Dyn. 11, 044502–44505. http://dx.doi.org/10.1115/1.4031197.
Harris, A.W., Fahnestock, E.G., Pravec, P., 2009. On the shapes and spins of "rubble pile" asteroids. Icarus 199, 310–318. http://dx.doi.org/10.1016/j.icarus.2008.09.012, URL: http://www.sciencedirect.com/science/article/pii/S0019103508003424.
Herique, A., Agnus, B., Asphaug, E., et al., 2018. Direct observations of asteroid interior and regolith structure: Science measurement requirements. Adv. Space Res. 62, 2141–2162. http://dx.doi.org/10.1016/j.asr.2017.10.020.
Herique, A., Plettemeier, D., Kofman, W., et al., 2019. A low frequency radar to fathom asteroids from Juventas Cubesat on HERA. In: EPSC-DPS Joint Meeting 2019, vol. 2019, pp. EPSC–DPS2019–807.
Hestroffer, D., Sánchez, P., Staron, L., et al., 2019. Small solar system bodies as granular media. Astron. Astrophys. Rev. 27, 6. http://dx.doi.org/10.1007/s00159-019-0117-5.
Hirabayashi, M., 2015. Failure modes and conditions of a cohesive, spherical body due to YORP spin-up. Mon. Not. R. Astron. Soc. 454, 2249–2257. http://dx.doi.org/10.1093/mnras/stv2017.
Hirabayashi, M., Nakano, R., Tatsumi, E., et al., 2020. Spin-driven evolution of asteroids' top-shapes at fast and slow spins seen from (101955) Bennu and (162173) Ryugu. Icarus 352, 113946. http://dx.doi.org/10.1016/j.icarus.2020.113946.
Hirabayashi, M., Sánchez, D.P., Scheeres, D.J., 2015. Internal structure of asteroids having surface shedding due to rotational instability. Astrophys. J. 808, 63. http://dx.doi.org/10.1088/0004-637x/808/1/63.
Hirabayashi, M., Tatsumi, E., Miyamoto, H., et al., 2019. The Western bulge of 162173 Ryugu formed as a result of a rotationally driven deformation process. Astrophys. J. 874, L10. http://dx.doi.org/10.3847/2041-8213/ab0e8b.
Ho, T.-M., Jaumann, R., Bibring, J.-P., et al., 2021. The MASCOT lander aboard Hayabusa2: The in-situ exploration of NEA (162173) Ryugu. Planet. Space Sci. 200, 105200. http://dx.doi.org/10.1016/j.pss.2021.105200.
Holsapple, K.A., 2004. Equilibrium figures of spinning bodies with self-gravity. Icarus 172, 272–303. http://dx.doi.org/10.1016/j.icarus.2004.05.023, Special Issue: Cassini-Huygens at Jupiter. URL: http://www.sciencedirect.com/science/article/pii/S0019103504001885.
Holsapple, K.A., 2007. Spin limits of solar system bodies: From the small fast-rotators to 2003 EL61. Icarus 187, 500–509. http://dx.doi.org/10.1016/j.icarus.2006.08.012, URL: http://www.sciencedirect.com/science/article/pii/S0019103506002776.
Hu, S., Richardson, D.C., Zhang, Y., Ji, J., 2021. Critical spin periods of sub-km-sized cohesive rubble-pile asteroids: Dependences on material parameters. Mon. Not. R. Astron. Soc. 502, 5277–5291. http://dx.doi.org/10.1093/mnras/stab412.
Jawin, E.R., Walsh, K.J., Barnouin, O.S., et al., 2020. Global patterns of recent mass movement on asteroid (101955) Bennu. J. Geophys. Res. Planets 125, http://dx.doi.org/10.1029/2020je006475.
Jutzi, M., Asphaug, E., Gillet, P., Barrat, J.-A., Benz, W., 2013. The structure of the asteroid 4 vesta as revealed by models of planet-scale collisions. Nature 494, 207–210. http://dx.doi.org/10.1038/nature11892.
Jutzi, M., Michel, P., Richardson, D.C., 2019. Fragment properties from large-scale asteroid collisions: I: Results from SPH/N-body simulations using porous parent bodies and improved material models. Icarus 317, 215–228. http://dx.doi.org/10.1016/j.icarus.2018.08.006.
Korycansky, D.G., Asphaug, E., 2006. Low-speed impacts between rubble piles modeled as collections of polyhedra. Icarus 181, 605–617. http://dx.doi.org/10.1016/j.icarus.2005.10.028, URL: http://www.sciencedirect.com/science/article/pii/S0019103505004422.
Korycansky, D.G., Asphaug, E., 2009. Low-speed impacts between rubble piles modeled as collections of polyhedra, 2. Icarus 204, 316–329. http://dx.doi.org/10.1016/j.icarus.2009.06.006, URL: http://www.sciencedirect.com/science/article/pii/S0019103509002516.
Lauretta, D.S., DellaGiustina, D.N., Bennett, C.A., et al., 2019a. The unexpected surface of asteroid (101955) Bennu. Nature 568, 55–60. http://dx.doi.org/10.1038/s41586-019-1033-6.
Lauretta, D.S., Hergenrother, C.W., Chesley, S.R., et al., 2019b. Episodes of particle ejection from the surface of the active asteroid (101955) Bennu. Science 366, eaay3544. http://dx.doi.org/10.1126/science.aay3544, URL: https://science.sciencemag.org/content/366/6470/eaay3544, arXiv:https://science.sciencemag.org/content/366/6470/eaay3544.full.pdf.
Leinhardt, Z.M., Richardson, D.C., Quinn, T., 2000. Direct N-body simulations of rubble pile collisions. Icarus 146, 133–151. http://dx.doi.org/10.1006/icar.2000.6370, URL: http://www.sciencedirect.com/science/article/pii/S001910350096370X.
Leisner, A.M., Richardson, D.C., Statler, T.S., Nichols, W., Zhang, Y., 2020. An extended parameter space study of the effect of cohesion in gravitational aggregates through spin-up simulations. Planet. Space Sci. 182, 104845. http://dx.doi.org/10.1016/j.pss.2020.104845, URL: http://www.sciencedirect.com/science/article/pii/S0032063318303180.
Mazhar, H., Heyn, T., Pazouki, A., et al., 2013. CHRONO: A parallel multi-physics library for rigid-body, flexible-body, and fluid dynamics. Mech. Sci. 4, 49–64. http://dx.doi.org/10.5194/ms-4-49-2013, URL: https://www.mech-sci.net/4/49/2013/.
Michel, P., Ballouz, R.-L., Barnouin, O.S., et al., 2020. Collisional formation of top-shaped asteroids and implications for the origins of Ryugu and Bennu. Nature Commun. 11, 2655. http://dx.doi.org/10.1038/s41467-020-16433-z.
Michel, P., Benz, W., Richardson, D.C., 2003. Disruption of fragmented parent bodies as the origin of asteroid families. Nature 421, 608–611. http://dx.doi.org/10.1038/nature01364.
Michel, P., Benz, W., Tanga, P., Richardson, D.C., 2001. Collisions and gravitational reaccumulation: Forming asteroid families and satellites. Science 294, 1696–1700. http://dx.doi.org/10.1126/science.1065189, URL: http://science.sciencemag.org/content/294/5547/1696.
Michel, P., Kueppers, M., Sierks, H., et al., 2018. European component of the AIDA mission to a binary asteroid: Characterization and interpretation of the impact of the DART mission. Adv. Space Res. 62, 2261–2272. http://dx.doi.org/10.1016/j.asr.2017.12.020.
Morota, T., Sugita, S., Cho, Y., et al., 2020. Sample collection from asteroid (162173) Ryugu by Hayabusa2: Implications for surface evolution. Science 368, 654–659. http://dx.doi.org/10.1126/science.aaz6306.
Murdoch, N., Sánchez, P., Schwartz, S.R., Miyamoto, H., 2015. Asteroid Surface Geophysics. University of Arizona Press, http://dx.doi.org/10.2458/azu_uapress_9780816532131-ch039.
Naidu, S.P., Benner, L.A.M., Brozovic, M., et al., 2020. Radar observations and a physical model of binary near-earth asteroid 65803 DIDYMOS, target of the DART mission. Icarus 348, 113777. http://dx.doi.org/10.1016/j.icarus.2020.113777, URL: http://www.sciencedirect.com/science/article/pii/S0019103520301640.
Nolan, M.C., Howell, E.S., Scheeres, D.J., et al., 2019. Detection of rotational acceleration of Bennu using HST light curve observations. Geophys. Res. Lett. 46, 1956–1962. http://dx.doi.org/10.1029/2018GL080658.
Paolicchi, P., Burns, J.A., Weidenschilling, S.J., 2002. Side effects of collisions: Spin rate changes, tumbling rotation states, and binary asteroids. In: Bottke, Jr., W.F., Cellino, A., Paolicchi, P., Binzel, R.P. (Eds.), Asteroids III. pp. 517–526.
Pazouki, A., Kwarta, M., Williams, K., et al., 2017. Compliant contact versus rigid contact: A comparison in the context of granular dynamics. Phys. Rev. E 96, 042905. http://dx.doi.org/10.1103/PhysRevE.96.042905.
Pravec, P., Scheirich, P., Kušnirák, P., et al., 2016. Binary asteroid population. 3. Secondary rotations and elongations. Icarus 267, 267–295. http://dx.doi.org/10.1016/j.icarus.2015.12.019.
Richardson, D.C., Michel, P., Walsh, K.J., Flynn, K.W., 2009. Numerical simulations of asteroids modelled as gravitational aggregates with cohesion. Planet. Space Sci. 57, 183–192. http://dx.doi.org/10.1016/j.pss.2008.04.015, Catastrophic Disruption in the Solar System. URL: http://www.sciencedirect.com/science/article/pii/S0032063308001037.
Roberts, J.H., Barnouin, O.S., Daly, M.G., et al., 2021. Rotational states and shapes of Ryugu and Bennu: Implications for interior structure and strength. Planet. Space Sci. 204, 105268. http://dx.doi.org/10.1016/j.pss.2021.105268.
Rozitis, B., MacLennan, E., Emery, J.P., 2014. Cohesive forces prevent the rotational breakup of rubble-pile asteroid (29075) 1950 DA. Nature 512, 174–176. http://dx.doi.org/10.1038/nature13632.
Rubincam, D.P., 2000. Radiative spin-up and spin-down of small asteroids. Icarus 148, 2–11. http://dx.doi.org/10.1006/icar.2000.6485.
Sánchez, P., 2015. Asteroid evolution: Role of geotechnical properties. Proc. Int. Astron. Union 10, 111–121. http://dx.doi.org/10.1017/s1743921315008583.
Sánchez, P., Scheeres, D.J., 2011. Simulating asteroid rubble piles with a self-gravitating soft-sphere distinct element method model. Astrophys. J. 727, 120, URL: http://stacks.iop.org/0004-637X/727/i=2/a=120.
Sánchez, P., Scheeres, D.J., 2014. The strength of regolith and rubble pile asteroids. Meteorit. Planet. Sci. 49, 788–811. http://dx.doi.org/10.1111/maps.12293.
Sánchez, P., Scheeres, D.J., 2018. Rotational evolution of self-gravitating aggregates with cores of variable strength. Planet. Space Sci. 157, 39–47. http://dx.doi.org/10.1016/j.pss.2018.04.001, URL: http://www.sciencedirect.com/science/article/pii/S0032063317304336.
Scheeres, D.J., French, A.S., Tricarico, P., et al., 2020. Heterogeneous mass distribution of the rubble-pile asteroid (101955) Bennu. Sci. Adv. 6, eabc3350. http://dx.doi.org/10.1126/sciadv.abc3350.
Scheeres, D.J., Hartzell, C.M., Sánchez, P., Swift, M., 2010. Scaling forces to asteroid surfaces: The role of cohesion. Icarus 210, 968–984. http://dx.doi.org/10.1016/j.icarus.2010.07.009, URL: http://www.sciencedirect.com/science/article/pii/S0019103510002812.
Scheeres, D.J., McMahon, J.W., French, A.S., et al., 2019. The dynamic geophysical environment of (101955) Bennu based on OSIRIS-REx measurements. Nature Astron. 3, 352–361. http://dx.doi.org/10.1038/s41550-019-0721-3.
Schwartz, S.R., Richardson, D.C., Michel, P., 2012. An implementation of the soft-sphere discrete element method in a high-performance parallel gravity tree-code. Granul. Matter 14, 363–380. http://dx.doi.org/10.1007/s10035-012-0346-z.

Sugita, S., Honda, R., Morota, T., et al., 2019. The geomorphology, color, and thermal properties of Ryugu: Implications for parent-body processes. Science 364, http://dx.doi.org/10.1126/science.aaw0422, URL: https://science.sciencemag.org/content/364/6437/eaaw0422.

Sugiura, K., Kobayashi, H., Watanabe, S., et al., 2021. SPH simulations for shape deformation of rubble-pile asteroids through spinup: The challenge for making top-shaped asteroids Ryugu and Bennu. Icarus 365, 114505. http://dx.doi.org/10.1016/j.icarus.2021.114505.

Tasora, A., Anitescu, M., 2010. A convex complementarity approach for simulating large granular flows. J. Comput. Nonlinear Dyn. 5, 031004–31010. http://dx.doi.org/10.1115/1.4001371.

Tasora, A., Serban, R., Mazhar, H., et al., 2016. Chrono: An open source multi-physics dynamics engine. In: Kozubek, T., Blaheta, R., Šístek, J., Rozložník, M., Čermák, M. (Eds.), High Performance Computing in Science and Engineering. Springer International Publishing, Cham, pp. 19–49.

Tricarico, P., Scheeres, D.J., French, A.S., et al., 2021. Internal rubble properties of asteroid (101955) Bennu. Icarus 114665. http://dx.doi.org/10.1016/j.icarus.2021.114665.

Walsh, K.J., Jawin, E.R., Ballouz, R.-L., et al., 2019. Craters, boulders and regolith of (101955) Bennu indicative of an old and dynamic surface. Nat. Geosci. 12, 242–246. http://dx.doi.org/10.1038/s41561-019-0326-6.

Walsh, K.J., Richardson, D.C., Michel, P., 2008. Rotational breakup as the origin of small binary asteroids. Nature 454, 188. http://dx.doi.org/10.1038/nature07078.

Watanabe, S., Hirabayashi, M., Hirata, N., et al., 2019. Hayabusa2 arrives at the carbonaceous asteroid 162173 Ryugu—A spinning top–shaped rubble pile. Science eaav8032. http://dx.doi.org/10.1126/science.aav8032.

Yu, Y., Michel, P., Hirabayashi, M., et al., 2018. The dynamical complexity of surface mass shedding from a top-shaped asteroid near the critical spin limit. Astron. J. 156, 59, URL: http://stacks.iop.org/1538-3881/156/i=2/a=59.

Zhang, Y., Lin, D.N.C., 2020. Tidal fragmentation as the origin of 1I/2017 U1 (‘Oumuamua). Nature Astron. http://dx.doi.org/10.1038/s41550-020-1065-8.

Zhang, Y., Michel, P., Richardson, D.C., et al., 2021. Creep stability of the DART/Hera mission target 65803 Didymos: II. the role of cohesion. Icarus 114433. http://dx.doi.org/10.1016/j.icarus.2021.114433.

Zhang, Y., Richardson, D.C., Barnouin, O.S., et al., 2018. Rotational failure of rubble-pile bodies: Influences of shear and cohesive strengths. Astrophys. J. 857, 15. http://dx.doi.org/10.3847/1538-4357/aab5b2.